Appl. Phys. B (2003)
DOI: 10.1007/s00340-003-1193-8

Applied Physics B
Lasers and Optics

Q. CAO[1,✉]
X. GU[1]
E. ZEEK[1]
M. KIMMEL[1]
R. TREBINO[1]
J. DUDLEY[2]
R.S. WINDELER[3]

Measurement of the intensity and phase of supercontinuum from an 8-mm-long microstructure fiber

[1] School of Physics, Georgia Institute of Technology, Atlanta, GA 30332-0430, USA
[2] Laboratoire d'Optique P.M. Duffieux, Université de Franche-Comté, 25030 Besançon cedex, France
[3] OFS Fitel Laboratories, 700 Mountain Avenue, Murray Hill, NJ 07974, USA

Received: 1 February 2003
Published online: 25 July 2003 •

ABSTRACT We generate, measure, and model broadband continuum generation from a relatively short 8-mm-long microstructure fiber pumped by 40-fs pulses at 816 nm in the near infrared. Cross-correlation frequency-resolved optical gating is used to measure the spectral intensity and phase of the output continuum, and the results are shown to be in good agreement with numerical simulations. The output temporal intensity exhibits a distinct series of ultra-short sub-40-fs-duration subpulses, with these results directly revealing for the first time the temporal pulse breakup and soliton fission that is the dominant initial spectral broadening process underlying supercontinuum generation in microstructure fibers.

PACS 42.65.Re; 42.81.Dp

1 Introduction

Although ultra-broadband supercontinuum (SC) can now be routinely generated using microstructure fibers (MFs) [1–10], its practical applications will require that we understand how best to create it. For example, what if we desire to generate the shortest possible continuum pulse? What if we wish to create the most stable continuum pulse? What if we wish to create continuum with the broadest possible spectrum? What if we wish to create continuum with the smoothest possible spectrum? Finding the answers to these questions will require detailed modeling and measurements of the continuum.

Recently, numerical simulations of SC generation, based on modified Maxwell or extended nonlinear Schrödinger equation (NLSE) models, have begun to improve our understanding of the underlying spectral broadening mechanisms involved [2–7]. In particular, although most of the reported SC generation experiments have been carried out using MF lengths in the range 10–100 cm, simulations have shown that the spectral broadening does not occur uniformly along the fiber length, and that significant spectral broadening occurs in only the first few millimeters of propagation due to the fission of the incident pulse into a series of constituent fundamental solitons [2, 5–7]. After this initial evolution phase, additional nonlinear effects such as the Raman self-frequency shift do introduce some additional spectral broadening, but this is relatively minor, and the main result of increased propagation distance is to temporally broaden the continuum [5].

Despite its obvious importance in the SC generation process, the detailed study of the spectral and temporal evolution of injected femtosecond pulses in MFs over the first few millimeters of propagation has not been the subject of any detailed experimental study. A correct understanding of this initial spectral broadening regime is crucial to improving the SC stability and for the optimization of the SC temporal and spectral properties for particular applications. While SC generation from a 4-mm photonic-crystal fiber (PCF) has been reported [10], it involved only measurements of its spectrum. The purpose of this paper is to describe the first intensity-and-phase measurements of continuum generated in this propagation regime, where we have injected 40-fs pulses at 816 nm into a sample of MF only 8-mm long. The MF output has been characterized using cross-correlation frequency-resolved optical gating (XFROG), which allows retrieval of the temporal and spectral intensity and phase of the SC for direct comparison with simulations. Our results directly reveal the temporal signatures of the soliton-fission process that is the dominant initial spectral broadening process underlying SC generation.

2 Numerical simulations for 15-cm propagation

We first review the results of previously published simulations studying the spectral and temporal evolution as a function of propagation distance for a MF length of 15 cm [4]. A selection of these results is reproduced in Fig. 1a and b. Here, we have assumed 30-fs, 10-kW peak-power pulses injected into a 15-cm length of large-air-fill fraction MF with a zero-dispersion wavelength (ZDW) around 780 nm. The fiber parameters are based on the Lucent MF described in [1], which we note is also the fiber used in the experiments described in Sect. 3. The simulations were carried out using an extended NLSE that included higher-order nonlinearity and stimulated Raman scattering. More details of the numerical modeling can be found in [7].

As shown in Fig. 1, the initial stage of propagation is dominated by nearly symmetrical spectral broadening, most of which occurs within the first 10 mm. Strong temporal com-

✉ E-mail: gte457x@mail.gatech.edu

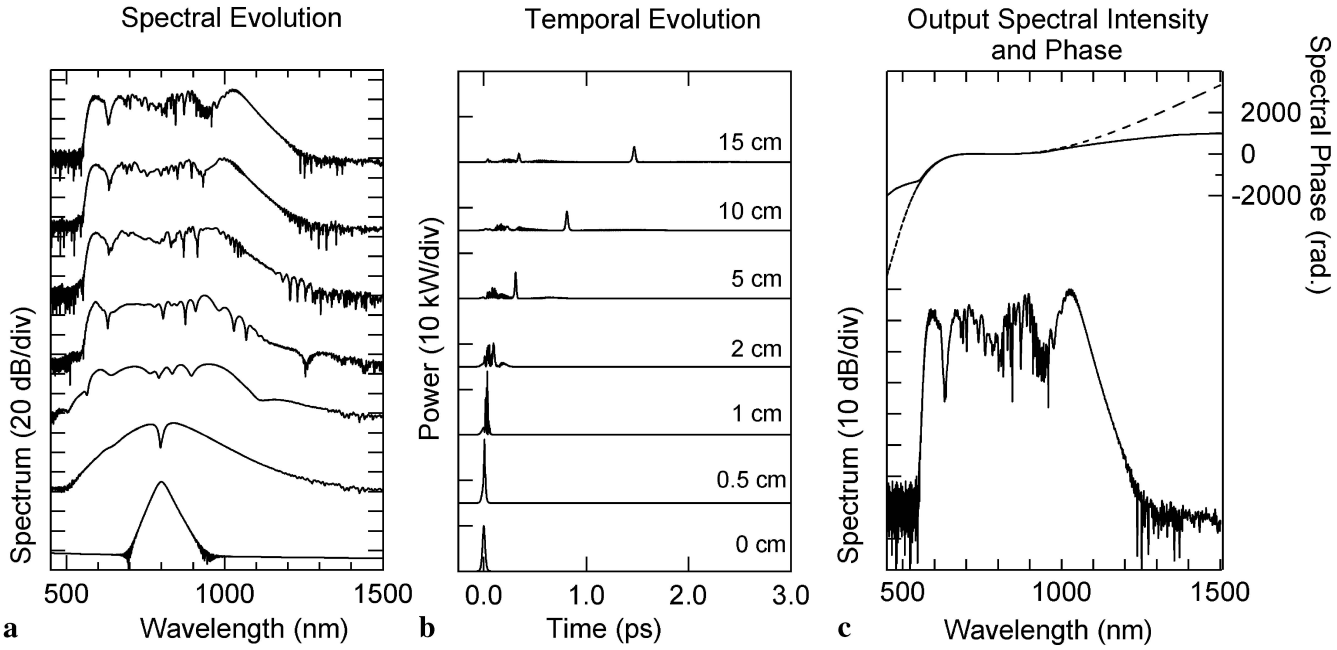

FIGURE 1 **a** Spectral and **b** temporal evolution in a microstructure fiber of an injected 10-kW peak power 30-fs input pulse injected at 800 nm, taken from [4]. **c** The output spectral intensity and phase (*solid line*) compared with the corresponding purely linear dispersive phase of the MF (*dashed line*)

pression also occurs over this range, but, after ~ 20 mm, the spectral broadening becomes strongly asymmetric and is associated with the development of more complex temporal features. Although the spectral broadening increases only slightly with further propagation, significant temporal broadening continues to occur due to the effect of linear dispersion acting on the generated broadband spectrum. In fact, after 15-cm propagation, the output spectral phase of the supercontinuum is dominated by the accumulated linear dispersion characteristics of the fiber, and there remain essentially no clear signatures of the initial strong nonlinear processes which have been responsible for the extreme spectral broadening. This is shown explicitly in Fig. 1c, where we again plot the output spectral intensity from the simulations, but also show the corresponding output spectral phase (solid line) and compare this with the spectral phase which would be expected based on purely linear propagation over the same distance in the fiber (dashed line). It is also clear that the supercontinuum spectral phase is predominantly cubic and, indeed, this observation is consistent with the results of previous XFROG measurements, which have clearly shown the parabolic group delay (and hence cubic spectral phase) characteristics of the SC [4].

3 Short-fiber continuum measurement and simulation

3.1 *Experimental setup*

The simulation results above suggest that a complete understanding of the initial nonlinear SC spectral broadening processes cannot be obtained from measurements made on SC generated in fiber lengths exceeding several centimeters. Therefore, in order to study the initial evolution phase, we have performed experiments in which femtosecond pulses have been injected into carefully prepared sub-centimeter-length fiber segments. A schematic diagram of our apparatus is shown in Fig. 2. Our pump laser was a KM Labs Ti:sapphire laser, which emitted a 100-MHz train of 40-fs pulses with an energy of about 2 nJ. The laser was not tunable, but its output wavelength of 816 nm is in the anomalous-dispersion regime of the Lucent MF used, so that comparable evolution characteristics to those in Fig. 1 would be expected. The input beam was then separated by a 50 : 50 beam splitter, so that half of it could be used as the reference pulse in XFROG measurements and the other half could be launched into an 8-mm length of Lucent MF. The reference pulse itself was measured using second-harmonic generation (SHG) FROG within half an hour of the XFROG measurement.

For our XFROG measurement, the output continuum was imaged using reflective optics and gated by the pump pulse itself in a 1-mm-thick BBO crystal, which achieved phase matching at all wavelengths by angle dithering with an amplitude of about 30°. While angle dithering the nonlinear crystal accounts for the phase mismatch due to group-velocity mismatch (GVM) between the input and signal pulses, GVM be-

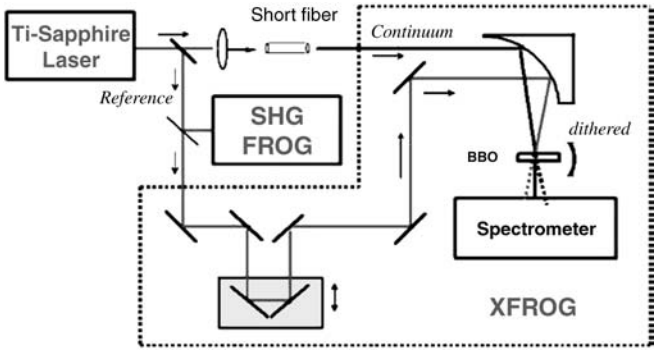

FIGURE 2 Experimental setup of the continuum XFROG measurement

tween the gate pulse and the continuum (the two input pulses) provides a limitation on our measurements. This results in a time smearing of the trace; we are developing code that takes this effect into account in future work.

Because the continuum has a very broad bandwidth, only reflective mirrors were used during the focusing. A 50-μm pinhole was used in the alignment to ensure that the continuum and gate pulses overlapped and were well focused in the crystal. The delay between the measured continuum and the gate pulse was scanned in 3.456-fs steps. The sum-frequency signal pulse generated by the continuum and gate beams was spectrally resolved at each delay. This yielded an XFROG trace of size 200×1024, which was then interpolated into a 256×256 trace for retrieval of the intensity and phase. The time-averaged continuum spectrum was also independently measured by an Ocean Optics spectrometer. The efficiency curve of the spectrometer used in the measurement was measured using a quartz tungsten halogen (QTH) calibration lamp, and the efficiency correction was applied to the measured trace before pulse retrieval. The wavelength-dependent phase-matching efficiency in the BBO crystal was also taken into account in our data pre-processing. After applying these corrections to our measured trace, the XFROG algorithm was then used for retrieval.

3.2 *SHG FROG measurement results of the reference pulse*

In addition to the XFROG measurement of the MF output, the intensity and phase of the reference pulse were characterized using (SHG) FROG [12, 13]. The results of these measurements are shown in Fig. 3. We note that the temporal FWHM of the pulse is about 40 fs and that there is a residual cubic spectral phase, which leads to strong trailing edge oscillations on the temporal intensity. We stress here that the reference pulse is also the fiber input pulse, so that its complete characterization is of critical importance for the accurate numerical modeling of the SC generation process.

3.3 *XFROG measurement results*

The squared magnitude of the spectrum of the cross-correlation signal recorded as a function of delay τ between the reference pulse and the measured pulse yields the XFROG trace or spectrogram [13]:

$$I_{\mathrm{XFROG}}^{\mathrm{SFG}}(\omega, \tau) = \left| \int_{-\infty}^{\infty} E(t) E_{\mathrm{Ref}}(t-\tau) \mathrm{e}^{-\mathrm{i}\omega t} \, \mathrm{d}t \right|^2 .$$

In previous work, we made XFROG measurements of the intensity and phase of the continuum from sub-100-fs pulses propagating through a many-cm-long fiber, which revealed a several-ps-long continuum, dominated by the linear optical (third-order dispersive) properties of the fiber [7, 11]. In addition, the continuum from this long fiber had much fine (~ 1 nm) spectral structure, yielding a time–bandwidth product in excess of 1000, requiring an 8192×8192 array and making the measurements difficult and the retrieval very slow. Worse (from the point of view of continuum applications and the meaning of the measurements), these XFROG measurements revealed that this structure was highly unstable.

Here, the continuum proves to be much shorter and more stable, significantly simplifying the measurements. Figure 4 shows the measured XFROG trace (left) and the retrieved trace (right) of the short-fiber continuum. We see from the figure that the retrieved trace is in good agreement with the measured one, reproducing all the major features. We attribute the additional structure that appears in the retrieved trace to shot-to-shot instability of spectral fine structure in the continuum spectrum as discussed in detail in [5].

The retrieved continuum intensity and phase vs. time (left) and frequency (right) are shown in Fig. 5. We note firstly

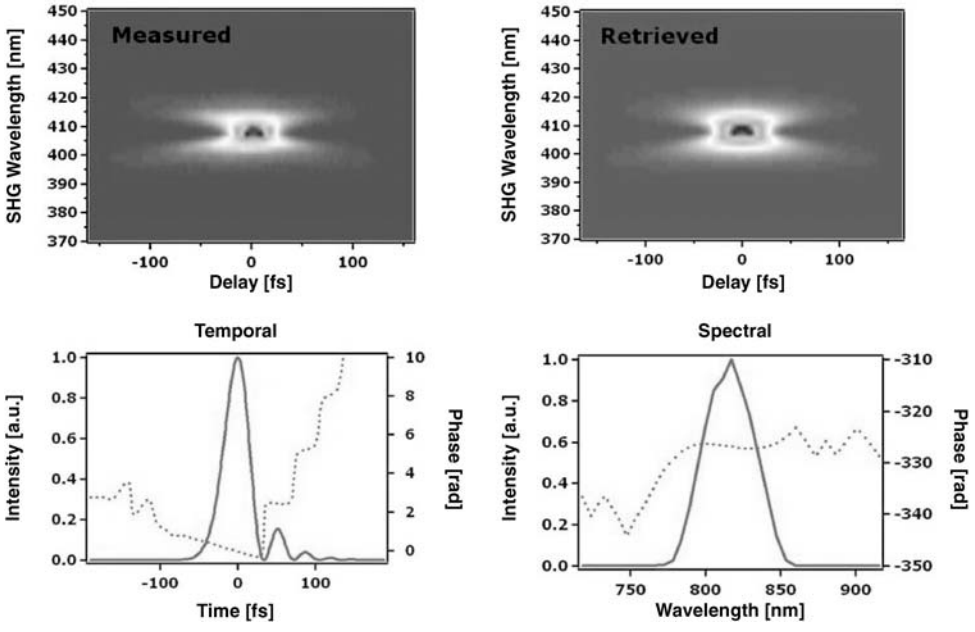

FIGURE 3 Experimental results of the SHG FROG measurement of the reference pulse

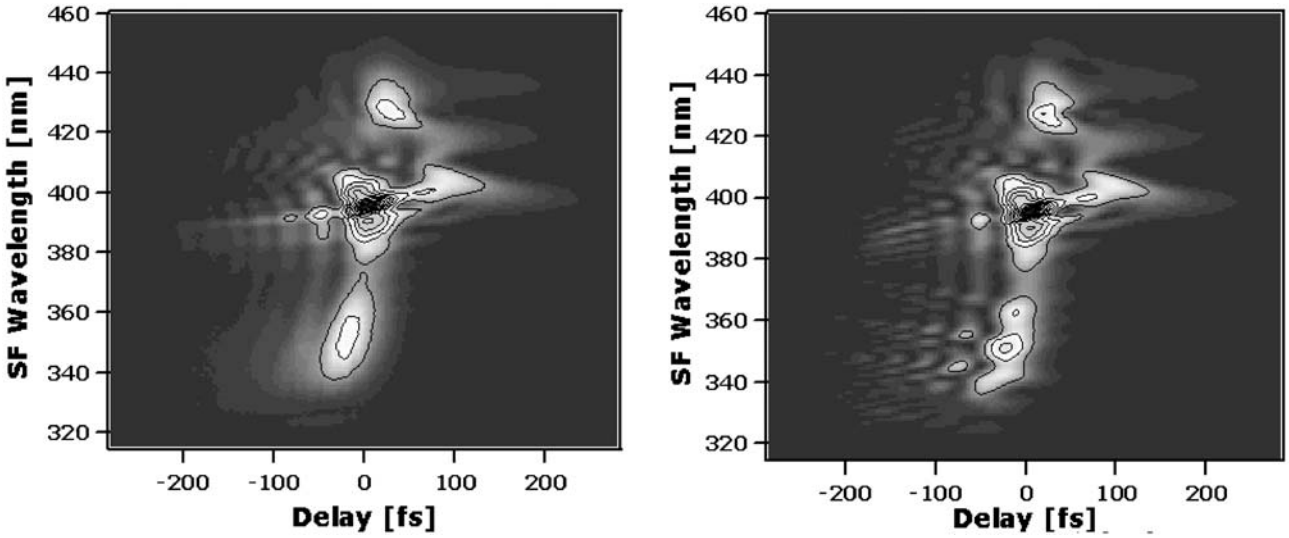

FIGURE 4 The measured XFROG trace (*left*) and the retrieved XFROG trace (*right*) of the 8-mm fiber continuum

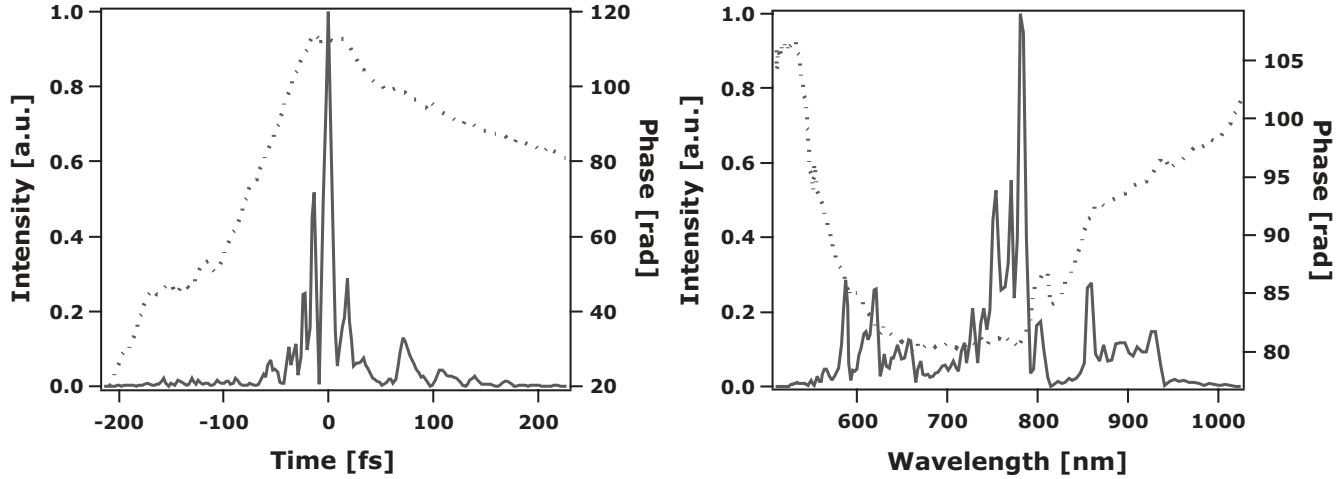

FIGURE 5 The retrieved continuum intensity and phase vs. time (*left*); the retrieved continuum intensity and phase vs. frequency (*right*). Note the shorter temporal extent of the continuum from the short fiber compared to the duration of the input pulse

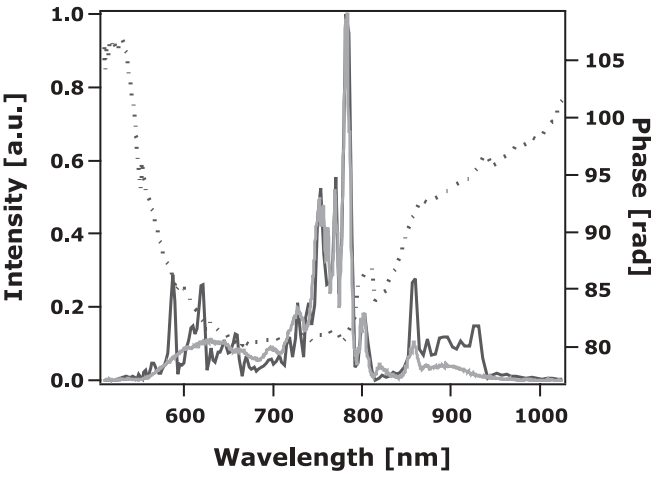

FIGURE 6 The retrieved continuum intensity and phase vs. frequency (*black*) and the independent measurement of the continuum spectrum (*gray*). Note the excellent agreement between the XFROG-measured spectrum and the independently measured spectrum (if we take into account the likely fluctuations in the spectrum from shot to shot)

that the temporal extent of the SC from the 8-mm-long MF is significantly shorter than the picosecond SC that is generated in a longer fiber and, indeed, consists of a series of sub-pulses that are shorter than the input 40-fs pulse. At the same time, the short-fiber continuum has less complex temporal and spectral features than the continuum pulses previously measured from longer fibers. The spectral phase of the short-fiber continuum is relatively flat, varying only around 25 rad, while the long-fiber continuum is dominated by a cubic phase spanning over 1000 π rad [11]. In view of the complexity of the SC, Fig. 6 shows that there is good agreement between the retrieved spectrum (black) and that independently measured using a spectrometer and averaged over $\sim 10^7$ pulses (gray). The discrepancies are due to shot-to-shot instabilities in the SC, which smear out the spectrometer-measured spectrum, as we discussed previously [11].

While the above continuum was quite short in time, it was not quite as broad in spectrum as the previously generated continuum from a microstructure fiber. This is likely due to a mismatch in the input laser wavelength and the fiber

zero-group-velocity-dispersion (GVD) wavelength, which we were unable to avoid. We confirmed this by generating continuum using the same laser wavelength and a longer piece of the same fiber and observing a similar continuum spectral width. Future work will involve use of a tunable fs source, emitting pulses at the fiber zero-GVD wavelength.

3.4 *Numerical simulations*

The extended NLSE model described in [7] was applied to study the initial period of evolution for the 8-mm MF samples used in the experiments described here. The simulation initial conditions of the input pulse's intensity and phase were based on the experimental input pulse parameters from SHG-FROG measurements as shown in Fig. 3, and the best experimental estimates available for the laser and fiber parameters. The intensity was adjusted so that it corresponded to an estimated pulse energy in the fiber core of 0.4 nJ (an estimated peak power of 8.6 kW). After 8 mm of propagation, the simulations yielded the temporal intensity shown in Fig. 7a and the spectral intensity shown in Fig. 7b (on a logarithmic scale) and Fig. 7c (on a linear scale). It is clear that there is very good qualitative agreement between experiment and simulation, with the differences attributed mainly to uncertainties in the fiber dispersion and in the injected power level in the fiber core, which are difficult to ascertain accurately with such a short fiber length. No systematic attempts were made to optimize the fit between experiment and simulation.

In order to gain further physical insight into the spectral broadening dynamics occurring during the 8 mm of propagation in the MF, we present in Fig. 8 the temporal and spectral evolution shown in 1-mm-propagation increments. The sig-

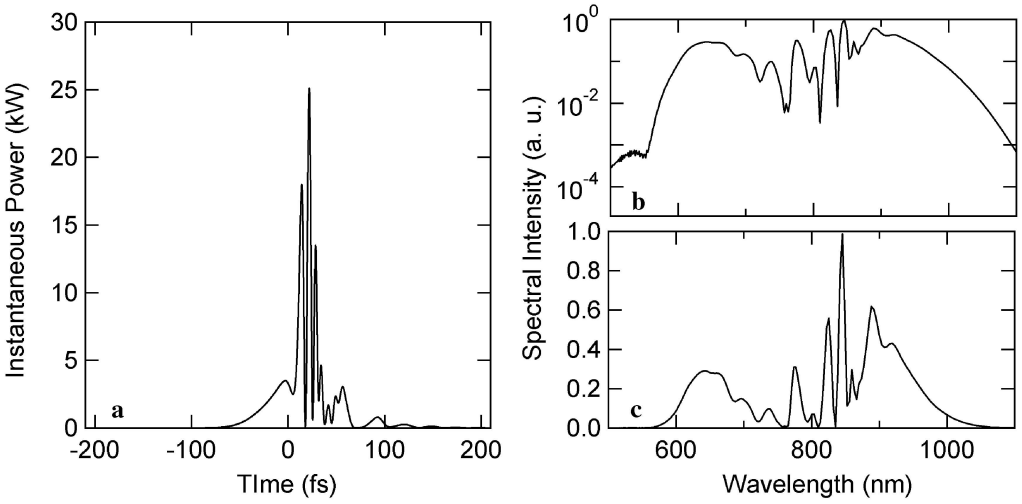

FIGURE 7 Simulation results showing **a** output temporal intensity, **b** output spectrum on a logarithmic scale, and **c** output spectrum on a linear scale

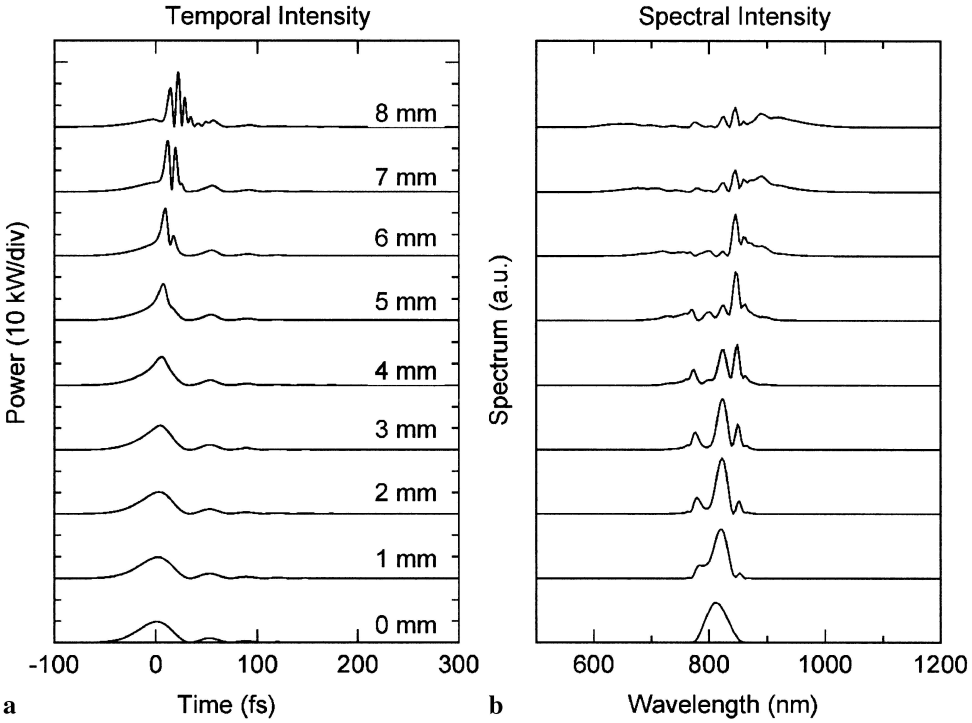

FIGURE 8 Simulation results showing evolution of **a** the temporal intensity and **b** the spectrum as a function of propagation distance

nificance of these results is that we clearly see the association of the initial spectral broadening with pulse splitting and breakup in the time domain, allowing the interpretation of our experimental intensity profile as showing the first direct temporal characterization of soliton-fission effects in microstructure fibers.

4 Conclusions

In conclusion, we have presented intensity-and-phase measurements that have demonstrated significant spectral broadening even over a short propagation distance in a microstructure fiber. Our XFROG measurement of the short-fiber continuum reveals that the temporal structure of the output continuum contains sub-pulses shorter than the input pulse that creates it. The experimental results have been compared with numerical simulations, with good qualitative agreement being obtained. Moreover, the simulations have allowed the temporal structure observed in experiments to be interpreted as due to soliton breakup or fission, which is the dominant spectral broadening mechanism present during the early stages of supercontinuum generation in microstructure fibers.

ACKNOWLEDGEMENTS This material is based upon wor supported by the National Science Foundation under Grant No. ECS-0200223. We thank Stéphane Coen and Alex Gaeta for many enjoyable and fruitful discussions.

REFERENCES

1 J.K. Ranka, R.S. Windeler, A.J. Stentz: Opt. Lett. **25**, 25 (2000)
2 A.L. Gaeta: Opt. Lett. **27**, 924 (2002)
3 S. Coen, A.H.L. Chau, R. Leonhardt, J.D. Harvey, J.C. Knight, W.J. Wadsworth, P.S.J. Russell: Opt. Lett. **26**, 1356 (2001)
4 S. Coen, A.H.L. Chau, R. Leonhardt, J.D. Harvey, J.C. Knight, W.J. Wadsworth, P.S.J. Russell: J. Opt. Soc. Am. B **19**, 753 (2002)
5 A.V. Husakou, J. Herrmann: Phys. Rev. Lett. **87**, 203 901 (2001)
6 J.M. Dudley, L. Provino, N. Grossard, H. Maillotte, R.S. Windeler, B.J. Eggleton, S. Coen: J. Opt. Soc. Am. B – Opt. Phys. **19**, 765 (2002)
7 J.M. Dudley, X. Gu, L. Xu, M. Kimmel, E. Zeek, P. O'Shea, R. Trebino, S. Coen, R.S. Windeler: Opt. Express **10**, 1215 (2002)
8 A.B. Fedotov, P. Zhou, Y.N. Kondrat'ev, S.N. Bagayev, V.S. Shevandin, K.V. Dukel'skii, A.V. Khokhlov, V.B. Smirnov, A.P. Tarasevitch, D. von der Linde, A.M. Zheltikov: Quantum Electron. **32**, 828 (2002)
9 A.B. Fedotov, A.N. Naumov, A.M. Zheltikov, I. Bugar, D. Chorvat, A.P. Tarasevitch, D. von der Linde: J. Opt. Soc. Am. B **19**, 2156 (2002)
10 A. Apolonski, B. Povazay, A. Unterhuber, W. Drexler, W.J. Wadsworth, J.C. Knight, P.S.J. Russell: J. Opt. Soc. Am. B **19**, 2165 (2002)
11 X. Gu, L. Xu, M. Kimmel, E. Zeek, P. O'Shea, A.P. Shreenath, R. Trebino, R.S. Windeler: Opt. Lett. **27**, 1174 (2002)
12 K.W. Delong, R. Trebino, J. Hunter, W.E. White: J. Opt. Soc. Am. B **11**, 2206 (1994)
13 R. Trebino (Ed.): *Frequency-Resolved Optical Gating: The Measurement of Ultrashort Laser Pulses* (Kluwer Academic, Boston 2002)